Surface-modified nanofibrous biomaterial bridge for the enhancement and control of neurite outgrowth

Nicole E. Zander[a)]
U.S. Army Research Laboratory, Weapons and Materials Research Directorate, Aberdeen Proving Ground, Maryland 21005 and Department of Chemistry and Biochemistry, University of Delaware, Newark, Delaware 19716

Joshua A. Orlicki and Adam M. Rawlett
U.S. Army Research Laboratory, Weapons and Materials Research Directorate, Aberdeen Proving Ground, Maryland 21005

Thomas P. Beebe, Jr.
Department of Chemistry and Biochemistry, University of Delaware, Newark, Delaware 19716

(Received 6 October 2010; accepted 22 November 2010; published 22 December 2010)

Biomaterial bridges constructed from electrospun fibers offer a promising alternative to traditional nerve tissue regeneration substrates. Aligned and unaligned polycaprolactone (PCL) electrospun fibers were prepared and functionalized with the extracellular matrix proteins collagen and laminin using covalent and physical adsorption attachment chemistries. The effect of the protein modified and native PCL nanofiber scaffolds on cell proliferation, neurite outgrowth rate, and orientation was examined with neuronlike PC12 cells. All protein modified scaffolds showed enhanced cellular adhesion and neurite outgrowth compared to unmodified PCL scaffolds. Neurite orientation was found to be in near perfect alignment with the fiber axis for cells grown on aligned fibers, with difference angles of less than 7° from the fiber axis, regardless of the surface chemistry. The bioavailability of PCL fibers with covalently attached laminin was found to be identical to that of PCL fibers with physically adsorbed laminin, indicating that the covalent chemistry did not change the protein conformation into a less active form and the covalent attachment of protein is a suitable method for enhancing the biocompatibility of tissue engineering scaffolds. © *2010 American Vacuum Society.* [DOI: 10.1116/1.3526140]

I. INTRODUCTION

The repair of both peripheral and central nervous system injuries remains a challenge in current medical research. Nearly 200 000 people in the U.S. suffer from a spinal cord injury each year.[1–3] Damaged axons in the central nervous system have a limited ability to regenerate due to the prolonged clearing of debris from the injury site and formation of the glial scar that suppresses neuronal regeneration.[4] In addition, gaps in the nerve tissue of the peripheral nervous system that is greater than 2 cm require some type of bridge in order to regain function.[5] The standard treatment for such injuries is an autograph in which nerve tissue is relocated from a donor site to the injury site. Although nerve tissue transplants can be highly effective, there are a number of limitations including the following: donor site morbidity, scarring, and the need for multiple operations.[6–8] In addition, full function of the tissue is seldom recovered.[4,9]

A major challenge is misdirected axonal growth, which can result in inappropriate re-enervation between axons and targets.[6] The two general approaches to control axonal outgrowth include the use of physical contact guidance cues such as topographical features and biochemical agents such as proteins and nerve growth factors. In the last several years, biomaterial bridges that are able to direct axonal growth across an injury site have gained much attention.[10,11] These bridges may be composed of guidance channels,[12] planar substrates such as microcontact printed proteins on glass or polymer films,[13] commercial polymer membranes,[14] hydrogels, or fibers.[15–18] Of these techniques, those with patterns with feature sizes less than a few hundred micrometers have been shown to efficiently direct axonal growth. Fibers are particularly attractive substrates as they can be highly aligned to provide directional guidance for neurite outgrowth. Recent research has demonstrated that fibers of similar size scale to cells or smaller (less than 30 μm), promote faster neurite outgrowth.[2,11] Thus, scaffolds with fibers in the nanometer regime could be advantageous.

Electrospinning is a technique that produces fibers with diameters in the range of tens of nanometers to several micrometers via high voltage and electrostatic and coulombic repulsive forces.[19,20] Electrospinning is an extremely versatile process in which a variety of synthetic and natural polymer fibers can be readily formed.[17] Fiber quality and diameter can be controlled by polymer solution concentration, solvent solution, flow rate, applied potential, and gap distance. Fiber alignment can be controlled by the collector design, with static collectors producing unaligned fibers and high speed take-up mandrels producing uniaxially oriented fibers.[21,22] Electrospun fibers are attractive candidates for biomaterial bridges due to their high surface area, porosity, and ease of alignment control. In addition, the fibrous struc-

a)Electronic mail: nicole.zander@arl.army.mil

ture and fiber diameters mimic the extracellular matrix (ECM), such as the collagen (CL) fibrils that range between 50 and 500 nm in diameter, enabling favorable cell-scaffold interaction.[23]

Although natural polymers such as collagen have been electrospun, due to the cost and ease of processing, most nanofibers produced for tissue engineering are synthetic. These fibers are generally hydrophobic and allow for only limited cellular adhesion.[24] Furthermore, synthetic fibers do not contain biochemical cues that interact with cells and influence cellular processes. Thus, it is highly desirable to modify the fibers to increase the biocompatibility of the scaffolds. There are a variety of methods to modify the fibers to increase hydrophilicity including acid or base treatments, plasma modification, and physical adsorption of proteins or other biomolecules.[25,26] In addition, several researchers have blended gelatin and other proteins into the electrospinning solution to form polymer-protein blends.[27–29] Of the aforementioned modifications, the incorporation of proteins onto the fibers has been the most beneficial in influencing cellular adhesion and processes. Although the incorporation of certain ECM proteins in and on electrospun nanofibers is known to be beneficial, and although other work has shown that fiber direction has a significant affect on neurite alignment, to the best of our knowledge, no study has directly compared two extracellular matrix proteins and their effect on neurite outgrowth on electrospun fibers whether aligned or unaligned.

In this work, the surface chemistry of covalent attachment versus physical adsorption, protein type, and fiber alignment affects of polycaprolactone (PCL) fibers on neuronlike PC12 cells were examined. Two extracellular matrix proteins, namely, collagen and laminin (LN), were compared in terms of their influence on PC12 cell neurite outgrowth length and orientation, cell adhesion, and proliferation. Collagen is the most prevalent structural protein of the ECM and contains the three-amino-acid sequence arginine-glycine-aspartic acid (RGD) binding sequence that reacts with integrin receptors on the growth cone and promotes cellular adhesion.[30] Laminin is a component of the basement membrane and contains the RGD sequence that aids in cell adhesion and the five-amino0acid sequence isoleucine-lysine-valine-alanine-valine (IKVAV) sequence that controls neurite outgrowth.[31] PC12 cells are derived from the phenochromocytoma of the rat adrenal medulla and undergo neuronlike differentiation when treated with nerve growth factor and thus allow the study of the effect of fiber orientation and surface chemistry on neurite outgrowth.[32]

II. EXPERIMENT

A. Materials

Polycaprolactone with an average molecular weight of 40 kDa was obtained from Polysciences, Inc. Anhydrous *N*,*N*-dimethylformamide (DMF), mouse laminin, bovine collagen type *I*, rabbit antilaminin, paraformaldehyde, Tween 20, *N*-(3-dimethylaminopropyl)-*N′*-ethylcarbondiimide (EDC), *N*-hydroxy succinimide (NHS), 2-(*N*-morpholino)ethanesulfonic acid (MES), and Triton X-100 were obtained from Sigma-Aldrich. Dichloromethane, Dulbecco modified eagle's medium (DMEM), calf serum, horse serum, trypsin-ethylenediamine tetraacetic acid, phosphate buffered saline (PBS), nerve growth factor (NGF 2.5S), and CellTiter 96® AQueous Assay (MTS) were obtained from Fisher Scientific. Rhodamine phalloidin and AlexaFluor® 488 donkey antirabbit IgG were obtained from Invitrogen.

B. Fabrication of electrospun fibers

A 20 wt % solution of PCL was prepared by dissolving PCL in a 50:50 (w/w) mixture of anhydrous DMF and dichloromethane and stirring at RT overnight. PCL fibers were electrospun using a custom built setup consisting of a syringe pump (Aladdin AL-1000) and a stationary aluminum plate (unaligned fibers) or a rotating 2 in. wide mandrel (aligned fibers). The mandrel was connected to a motor (Bodine NSH-12R) with a speed controller (Minarik Electric Company SH-14), allowing the mandrel to rotate between 0 and 8000 rpm. A 5 ml syringe was filled with polymer solution and fed through an 18 G stainless steel needle at flow rates of 1–5 ml/h with an applied potential of 18.5 kV. The gap between the needle and the collector was fixed at 7 in., and the collector was set to an applied potential of −3 kV. Fibers were dried under vacuum at RT overnight before characterization and functionalization.

C. Electrospun fiber modification

1. Covalent attachment of laminin and collagen onto nanofibers

Vacuum dried PCL fibers were cut to fit in 24-well plates and plasma treated in air using an inductively coupled radio frequency (rf) plasma cleaner (Harrick PDC-32-G) for 5 min at a rf power of 18 W to introduce carboxylic functionalities to the surface of the fibers. Plasma treated fibers were then immersed in a MES buffer containing 5 mg/ml EDC and 5 mg/ml NHS for 1 h at RT.[33] Fiber mats were then rinsed with MES buffer and incubated in a 50 μg/ml laminin or collagen solution overnight at 4 °C. The protein solution was removed and the mats were washed in a 0.05% Tween 20 solution in PBS with gentle shaking for 30 min to remove physically absorbed proteins. Mats were then washed thoroughly with PBS and sterilized overnight by immersing in a sterile solution of 2% antibiotic/antimycotic in PBS. Samples were kept sterile for cell culture studies or rinsed thoroughly with de-ionized water and dried for characterization.

2. Physical absorption of laminin and collagen onto nanofibers

Vacuum dried PCL fibers were cut to fit in 24-well plates and rinsed thoroughly with PBS. The fiber mats were then incubated in a 50 μg/ml laminin or collagen solution overnight at 4 °C. The protein solution was removed and the mats were then washed thoroughly with PBS and sterilized overnight by immersing in a sterile solution of 2% antibiotic/

antimycotic in PBS. Samples were kept sterile for cell culture studies or rinsed thoroughly with de-ionized water and dried for characterization.

D. Characterization of scaffolds

The morphology of the fiber scaffolds was examined using a field emission scanning electron microscopy (Hitachi S-4700) in the secondary electron mode using a mixture of upper and lower detectors. An accelerating voltage of 0.6 kV was maintained in order to prevent surface damage to the substrate. Before observation, the samples were first coated with gold using a sputter coater (Hummer XP sputtering system, Anatech Ltd.). Several areas were imaged in order to examine the uniformity of the fiber diameters and alignment. Fiber diameters were measured using image analysis software (IMAGE J, National Institutes of Health). Alignment of fibers was qualitatively determined using fast Fourier transforms (FFTs) calculated using IMAGE J software.

The wettability of the surface was determined using a sessile drop contact angle system (First Ten Ångstroms) with an RS170 camera. The contact angles were measured and calculated using an automated fitting program (FTA32 v2.0). All reported contact angles are the average of $n=5$ measurements on three replicated samples. De-ionized water was used to test the contact angle of the fiber mats (Milli-Q filtration system).

Surface compositional analysis was performed using a Kratos Axis Ultra 165 x-ray photoelectron spectroscopy (XPS) system equipped with a hemispherical analyzer. Sampling areas of 1×0.5 mm^2 were irradiated with a 100 W monochromatic Al $K\alpha$ (1486.7 eV) beam and take-off angle of 90°. The XPS chamber pressure was maintained between 10^{-9} and 10^{-10} Torr. Elemental high-resolution scans were conducted with a 20 eV pass energy for the C 1*s*, O 1*s*, and N 1*s* core levels. A value of 284.6 eV for the hydrocarbon C 1*s* core level was used as the calibration energy for the binding energy scale. Data were processed using CASA XPS software. All reported atomic percentages are the average of $n=2$ measurements on a minimum of three replicated samples.

Near surface chemical analysis was performed by attenuated total reflection-Fourier transform infrared (ATR-FTIR) spectroscopy (Thermo Nicolet Nexus 870 ESP) using 256 scans and 4 cm^{-1} resolution over a range of 4000–400 cm^{-1}. ATR-FTIR spectra were collected using a Specac IR sampling accessory with a germanium crystal in multibounce mode. FTIR data were processed by importing to CASA XPS software for peak fitting and integration.

E. Culture of PC12 cells

PC12 cells were cultured in high glucose DMEM supplemented with 10% heat inactivated horse serum, 5% calf serum, and 1% antibiotic/antimycotic (complete medium) at 37 °C and 5% CO_2. Sterile fiber mats in 24-well plates were incubated in medium 2 h prior to seeding cells. PC12 cells were seeded at a density of 10 000 cells/well in complete medium for cell viability assays. For differentiation studies, cells were seeded at a density of 5000 cells/well in DMEM with 1% horse serum, 0.5% calf serum, and 1% antibiotic/antimycotic (differentiation medium). After 24 h, 50 mg/ml NGF was added to the differentiation medium.

F. Neurite outgrowth study

After day 1, 3, and 5 of seeding cells in differentiation medium supplemented with NGF, neurite outgrowth was characterized by staining actin filaments with phalloidin and analyzing with confocal laser scanning microscopy (CLSM). To prepare samples for CLSM, the fiber scaffolds were rinsed thoroughly with PBS and fixed in 4% paraformaldehyde in PBS for 20 min. Scaffolds were rinsed with PBS, and cells were permeabilized with 0.2% Triton X-100 for 10 min. Nonspecific labeling was prevented by incubating samples in a blocking buffer composed of 3% bovine serum albumin (BSA) in PBS for 20 min. Samples were then immersed in rhodamine phalloidin (1:200) in blocking buffer for 1 h. Samples were rinsed thoroughly with PBS and kept in the dark at 4 °C until analysis.

Samples were imaged on a Zeiss LSM5 Pascal equipped with Epiplan-Neofluar lenses. The cells in the scaffolds were imaged with a 543 nm laser. For neurite orientation studies, the PCL fibers were imaged using a 488 nm laser in reflection mode to allow measurement of the orientation angle of the fibers and cells in a single image. These samples were imaged in multitrack mode in order to prevent cross-talk between the 543 and 488 nm laser channels. A minimum of $n=5$ random areas for each of three replicate samples were imaged using the 10× and 20× objectives. Neurite length and orientation of neurites and fibers were measured using the Zeiss LSM software.

Alignment of cells and neurites was also calculated using FFTs of CLSM images in the IMAGE J program. The oval plug-in was used to sum the pixel intensities along a circular projection on the FFT.[34] Pixel intensity and orientation data were processed by importing into CASA XPS software for peak fitting and integration. Full width at half maxima of the peaks were compared to determine the relative degree of alignment of the cells and neurites.

Fractional area coverage of cells was calculated by importing CLSM images into IMAGE J, setting a threshold and using the analyze particles feature.

G. Cell viability and proliferation assay

The viability and proliferation of PC12 cells on the fiber scaffolds were determined using a MTS assay after day 1, 3, and 7 of culture in a complete medium. After the specified time point, the medium was removed and the cell-seeded scaffolds were transferred to a clean 24-well plate. Clear serum-free DMEM (400 μl) and MTS solution (100 μl) were added to each well. The samples were covered in foil and incubated at 37 °C for 3 h. A 150 μl aliquot from each sample was removed and transferred to a 96-well plate to be analyzed with a spectrophotometric plate reader (Perkin Elmer Fusion). Controls of each sample type without cells

were also analyzed to calculate background absorbance values for correction. The absorbance at 490 nm was recorded for each well for $n=4$ replicates for each sample and time point. In order to determine the number of viable cells, a calibration of known concentrations of PC12 cells in solution was conducted. All values were corrected for background absorbance and normalized to PC12 cells grown for 1 day on tissue culture polystyrene.

H. Polyclonal bioavailability assay

The bioavailability of the PCL fibers with covalently attached laminin and physically adsorbed laminin was as probed by a laminin polyclonal antibody and evaluated using a fluorescent immunoassay. Samples were prepared and rinsed as previously described. Samples were then immersed in a blocking buffer (3% BSA in 10% donkey serum) to minimize nonspecific adsorption. Samples were then incubated in a rabbit antilaminin antibody (1:200) in blocking buffer overnight at 4 °C. Subsequently, the samples were washed and incubated in AlexaFluor® 488 donkey antirabbit secondary antibody (1:200) for 1 h at RT. The immunostained samples were imaged using CLSM microscopy on a Zeiss LSM5 Pascal. Detector gain and amplifier offset were kept constant for all samples to enable semiquantitative comparison. Unmodified PCL fiber controls as well as controls to determine the nonspecific attachment of the secondary antibody and the autofluorescence of primary antibody and sample were also evaluated. A minimum of $n=5$ random areas for each of three replicate samples were imaged using the 20× objective. The mean intensity was determined using the Zeiss LSM software histogram feature.

I. Statistics

All data are expressed as mean ± standard error of the mean unless noted. One-way analysis of variance with *post hoc* Tukey means comparison tests and unpaired Student's *t*-tests were conducted with a significance level of $p<0.05$. A minimum of three replicate samples were used for all experiments.

III. RESULTS AND DISCUSSION

A. Morphology and chemical characterization of nanofibrous scaffolds

The electrospinning technique was utilized to fabricate PCL scaffolds composed of fibers with diameters between 100 and 800 nm. Figure 1 displays scanning electron micrographs of random and aligned PCL fibers and their respective fiber diameter distribution (inset). As can be seen from the histograms, the aligned fibers had significantly smaller diameters [260 ± 120 nm, ($n=50$)] compared to the unaligned fibers [530 ± 360 nm, ($n=50$)], as has been reported previously (mean ± SD).[35] In addition, the width of the size distribution for aligned fibers was narrower, indicating more uniform fibers. As evidenced by our results and literature precedence, fiber diameter and uniformity, as well as fiber orientation, can be tailored by rotation speed, as well as other processing parameters such as polymer concentration.[16,17] Faster rotation speeds lead to more uniform drawing of the fibers and hence less variation in fiber diameter. However, rotation speeds faster than the drawing speed of the fibers, can cause broken fibers. Thus, for this work, we found that a 5000 rpm rotation speed for a 20 wt % PCL solution was optimal for generating highly aligned fibers with reproducible fiber diameters and small size distributions.

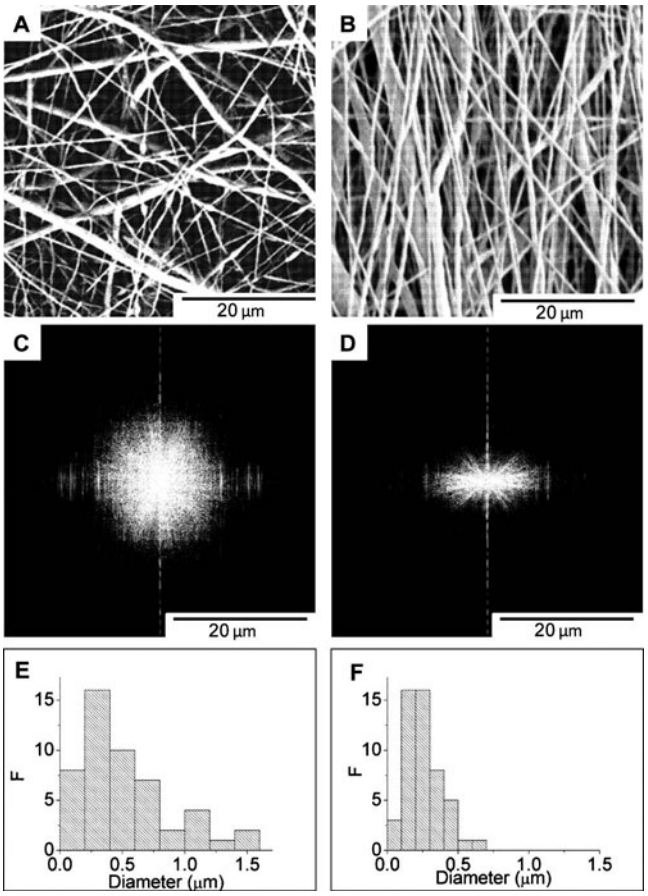

FIG. 1. Scanning electron micrographs and FFTs of electrospun PCL fibers. (a) Unaligned PCL fibers, (b) aligned PCL fibers, (c) FFT of (a), (d) FFT of (b), (e) histogram of (a) ($n=50$), and (f) histogram of (b) ($n=50$). The FFT of (b) indicates that the fibers are uniaxially aligned, whereas the FFT of (a) suggests no principal axis of alignment. Note different scales and narrower size distribution of aligned fibers.

A qualitative measure of fiber alignment was determined using FFTs, as displayed in Fig. 1. For the unaligned fibers, the FFT pattern was spherical, indicating that the pixel intensity was uniform in all directions or that there was no principal axis of fiber orientation. The FFT for the aligned fibers displayed an elliptical band perpendicular to the principal fiber axis. Although there was evidence of some misaligned fibers shown by the small radial FFT bands, the FFT pattern indicated a high degree of fiber alignment.

Although the plasma treatment of surfaces alone has been shown to increase cellular adhesion, cellular differentiation and proliferation were further enhanced by soaking the plasma-treated surfaces in protein.[36,37] Thus, in order to enhance the adhesion and differentiation of PC12 cells on the

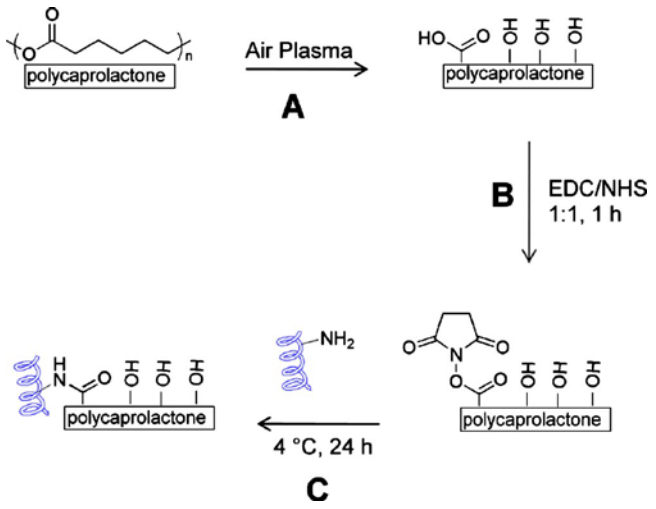

FIG. 2. (Color onlne) Schematic of covalent coupling reaction for the attachment of protein to PCL fibers. (a) Air plasma treatment of PCL fibers resulting in oxidized forms of carbon at the fiber surface. (b) Attachment of NHS via EDC coupling reaction (5 mg/ml, 1:1). (c) Attachment of protein through reaction with amine groups.

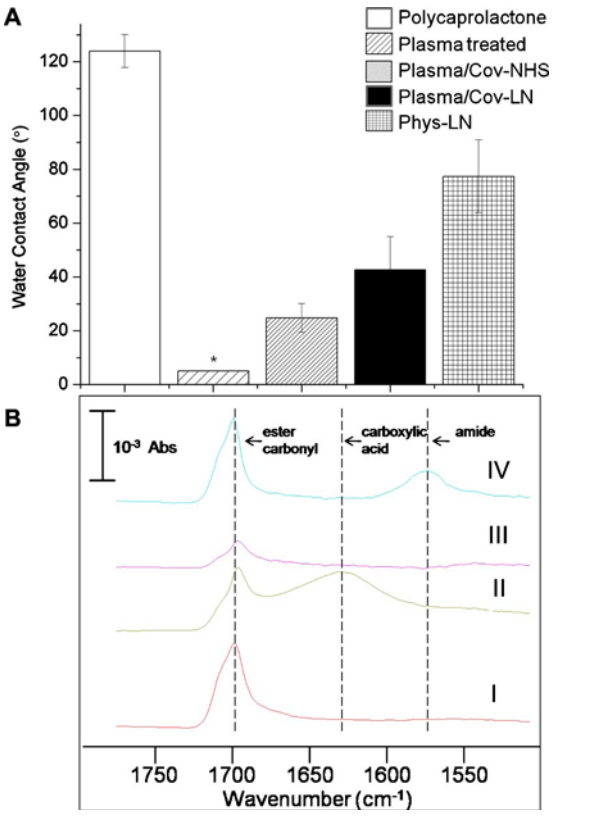

FIG. 3. (Color onlne) (a) Sessile-drop water contact angle of electrospun PCL fiber mats with the following surface chemistries: (left to right) unmodified, plasma-treated, plasma-treated with covalently attached *N*-hydroxy succinimide (plasma/cov-NHS), plasma-treated with covalently attached laminin (plasma/cov-LN), and physically adsorbed laminin (phys-LN). (* contact angle $<5°$). Error bars represent mean $\pm$ standard error of the mean, $n=15$. (b) FTIR-ATR spectra of electrospun PCL fibers: (i) as-spun with no surface modification, (ii) plasma-treated PCL fibers, (iii) plasma-treated PCL fibers with covalently attached *N*-hydroxy succinimide, and (iv) plasma-treated PCL fibers with covalently attached collagen. Dashed lines denote positions of peaks of interest.

nanofibers, proteins were attached to the fibers using two methods. In the first method shown in Fig. 2, the nanofibers were air plasma treated to introduce carboxylic acid groups on the surface. The carboxylic groups were then activated with EDC and NHS and coupled to the protein. Both ECM proteins collagen and laminin were coupled using this chemistry to determine if different binding domains in the proteins would influence the cells to grow or differentiate at different rates. As laminin contains a binding sequence that influences neurite outgrowth, it was expected that longer neurites would be observed on these samples. In order to compare the effects of attachment chemistry in terms of surface protein coverage, a second method in which the proteins were physically adsorbed to the nanofibers was also examined. In this method, the fibers were not plasma treated and thus remained hydrophobic.

The wettability of the PCL fibers and fibers with attached protein was probed using contact angle. The advancing water contact angle results for native and functionalized PCL fibers are displayed in Fig. 3(a). The unmodified PCL fibers were extremely hydrophobic with a contact angle of approximately 120° due to hydrophobic backbone of the polymer and the high surface roughness of the nanometer sized fibers. After 5 min of air plasma treatment, the fibers became significantly wettable due to the introduction of hydroxyl and other polar functional groups that a contact angle could not be measured. Attachment of NHS increased the contact angle to approximately 25° and covalent attachment of laminin further increased the contact angle to approximately 40°. A contact angle of approximately 80° was observed for PCL with physically adsorbed laminin, which was significantly higher than the covalently attached laminin surface as the former fibers were not plasma treated but substantially reduced compared to the unmodified PCL due to the hydrophilic functionalities on the protein. Contact angles were similar for collagen modified surfaces.

The chemical composition of the fiber mats was examined using FTIR-ATR, which gives molecular information about the top 1–5 μm of the material. Figure 3(b) displays FTIR-ATR spectra for each step in the covalent modification process: native PCL, plasma-treated PCL, PCL with covalently attached NHS, and PCL with covalently attached protein. After plasma treatment, a carboxylic acid stretch at 1630 cm^{-1} became evident. After protein attachment, the carboxylic acid band disappeared and an amide II band became apparent at 1580 cm^{-1}, indicating consumption of the carboxylic acid groups on the fiber surface and formation of amide bonds with the protein. Component fitting of the carbonyl peak at approximately 1704 cm^{-1} revealed similar information as described above. The carboxyl component increased from 33.7 to 79.3 at. % after PCL was treated with plasma. After attachment of NHS, the carboxyl component was replaced with amide and imide components.

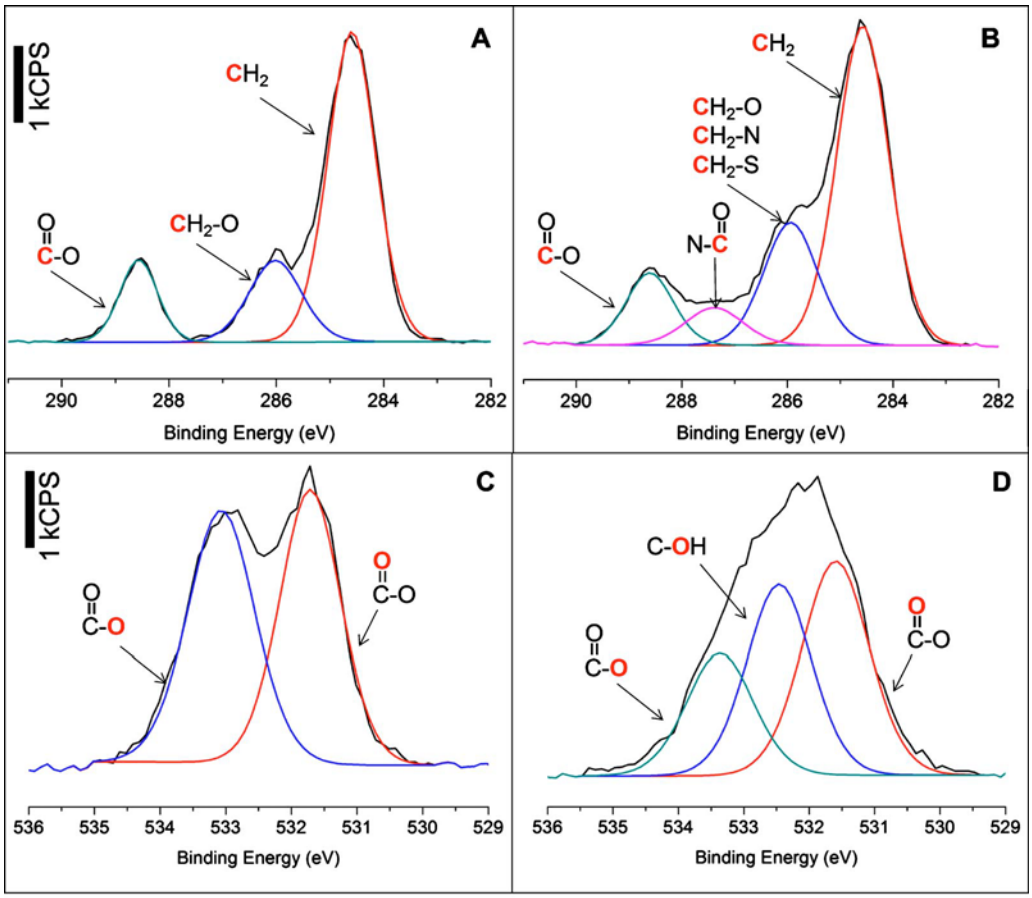

E Surface Chemistry	XPS atomic percentage		
	Carbon	Oxygen	Nitrogen
Nominal PCL	75	25	-
PCL melt-pressed film	78.5 ± 0.3	21.5 ± 0.3	-
PCL electrospun fibers	80.8 ± 0.6	19.1 ± 0.8	-
After plasma treatment	71.8 ± 1.0	28.2 ± 0.9	-
After reaction with NHS	63.1 ± 1.8	35.8 ± 2.4	1.1 ± 0.5
PCL w/ covalently attached laminin	70.8 ± 2.2	22.0 ± 1.3	7.2 ± 0.8
PCL w/ physisorbed laminin	70.5 ± 2.5	23.2 ± 0.9	6.3 ± 1.6
PCL w/ covalently attached collagen	72.6 ± 2.5	25.4 ± 2.5	2.0 ± 0.3
PCL w/ physisorbed collagen	71.0 ± 2.0	21.6 ± 1.7	7.4 ± 0.6

FIG. 4. (Color onlne) High-resolution x-ray photoelectron spectra of electrospun PCL fibers. (a) C 1*s* of unmodified PCL fibers, (b) C 1*s* of plasma-treated PCL fibers with covalently attached laminin, (c) O 1*s* of unmodified PCL fibers, (d) O 1*s* of plasma-treated PCL fibers, and (e) atomic composition of native and modified PCL nanofibers as determined by x-ray photoelectron spectroscopy, mean ± standard deviation ($n=6$). Weakly bound physically absorbed proteins were removed with gentle shaking in a 0.05% Tween 20 solution (mats with covalent chemistry only) and rinsing with PBS.

The surface chemistry of the fibers was probed with XPS in order to gain an understanding of the portion of the fiber mats in contact with the cells. Atomic compositions of the PCL fibers [Fig. 4(e)] showed an increase in oxygen after plasma treatment, an addition of nitrogen after the NHS reaction, and an increase in nitrogen after protein attachment, confirming the attachment of laminin and collagen proteins (both covalent and physically adsorbed). For the protein laminin, the coverage difference between the physically adsorbed and covalently attached samples was not statistically significant ($p<0.05$). This is also seen in the table for the *N* percentage. The at. % nitrogen for the nanofibers with physically adsorbed collagen was similar to the fibers with laminin, but the at. % nitrogen on covalently attached collagen was significantly lower.

The high-resolution C 1*s* spectra of unmodified PCL and PCL with covalently attached laminin are displayed in Figs. 4(a) and 4(b). PCL has three components consisting of the hydrocarbon (67.1%), ether of the ester (19.1%), and carboxylic (13.8%). Attachment of the protein introduced a fourth component for the amide bond (8.4%) formed in the reaction in addition to the hydrocarbon (47.7%), ether of the ester and hydroxyl (35.8%), and carboxylic (8.0%) components. Figures 4(c) and 4(d) display the high-resolution O 1*s*

spectra for native PCL and plasma-treated PCL nanofibers. The unmodified PCL fiber O 1*s* consisted of the carbonyl *O* and ester *O* components in a near 50:50 ratio. After plasma treatment, the O 1*s* contained a third hydroxyl component (35.5%), with the carbonyl and ester *O* compositions being reduced to 41.0% and 23.5%, respectively.

The bioavailability of the PCL fibers with covalently attached laminin and physically adsorbed laminin was as probed by a laminin polyclonal antibody and evaluated using a fluorescent immunoassay (see supplemental data, Fig. 1).[38] Identical intensity histograms were observed for both protein attachment methods, indicating that similar concentrations of the polyactive forms of laminin were presented to the polyclonal antilaminin antibody for both protein attachment methods.

B. Interaction of PC12 cells with aligned PCL nanofibrous scaffolds

The addition of proteins, ECM proteins in particular, have been shown to increase cellular adhesion and aid in cellular processes. In this work, two ECM proteins, namely, collagen and laminin, were evaluated for their efficacy in improving cellular adhesion, proliferation, and differentiation of neuronlike PC12 cells on PCL nanofibrous scaffolds. Before conducting differentiation studies, the viability and proliferation of PC12 cells on the native and modified PCL fibers were evaluated with a standard MTS assay which correlated absorbance with the number of viable cells (see supplemental data, Fig. 2).[38] The viability was highest on day 1 for native PCL fibers, which may have been due to a cell-scaffold interaction on the protein modified surfaces that temporarily slowed cell growth, but the number of viable cells increased from day 1 to day 7 for all scaffold surfaces. Although the protein modified fibers did not have significantly higher viability as expected, the results showed that PC12 cells are at least as viable on protein modified scaffolds as on native PCL and that these scaffolds are suitable substrates for supporting cell growth.

After verifying the viability of PC12 cells on the PCL scaffolds, the neurite outgrowth was examined in order to understand how different surface chemistries and fiber orientations affect neurite extension rates and orientation, as well as cellular elongation. Figures 5(a)–5(e) display CLSM micrographs of PC12 cells grown for 5 days on the different surfaces examined, in which cellular and neurite elongation in the direction of the fiber axis is clearly evident. Figure 5(f) displays neurite lengths for days 1, 3, and 5 for cells cultured on native and modified PCL fibers as well as the area fraction of cell coverage calculated from CLSM microscopy images. All fibers treated with protein enhanced neurite outgrowth when compared to native PCL fibers. Area fraction coverage or adhesion of cells was also significantly improved on fibers with protein (15%–20% coverage) compared to unmodified PCL fibers (3%). In addition, cells grown on all fibers, except those with covalently attached collagen, had significantly longer neurites on day 5 when compared to day 3 for the same material. Cells grown on fibers with covalent collagen had significantly shorter neurites on day 5 than those grown on fibers with laminin and physically adsorbed collagen. The reduced neurite outgrowth on PCL fibers with covalently attached collagen could be attributed to lower concentration of protein on the surface when compared to the other protein modified fibers (based on reduced at. % nitrogen from XPS data). The lower efficiency of the collagen covalent coupling reaction compared to laminin can likely be ascribed to the lower *p*H conditions of the reaction, *p*H 5 for the former and *p*H 8 for the latter, which reduced the nucleophilicity of the primary amines on the protein.

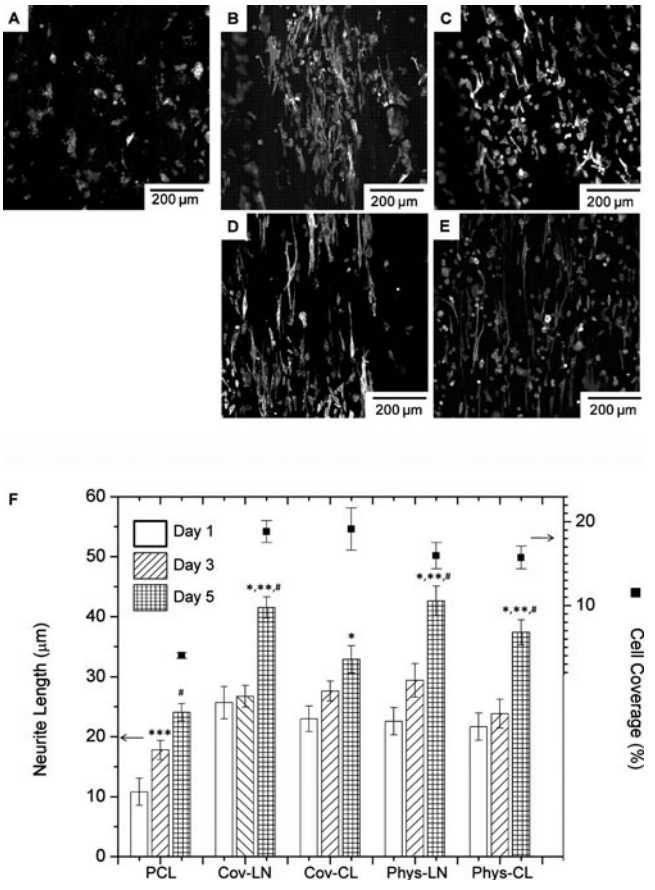

FIG. 5. [(a)–(e)] Confocal scanning laser microscopy images of PC12 cells on aligned electrospun PCL fibers. (a) Unmodified PCL fibers, (b) plasma-treated PCL fibers with covalently attached laminin, (c) plasma-treated PCL fibers with covalently attached collagen, (d) PCL fibers with physically adsorbed laminin, and (e) PCL fibers with physically adsorbed collagen. (f) Neurite outgrowth of PC12 cells cultured on electrospun PCL fibers with physically adsorbed and covalently attached LN and CL. Data are expressed as mean ± standard error of the mean ($n=3$) ($^{*}p<0.05$ compared to day 5 PCL fibers, $^{**}p<0.05$ compared to day 5 covalent-CL fibers, $^{***}p<0.05$ compared to day 1 PCL fibers, and $^{\#}p<0.05$ compared to day 3 fibers of same material). Right axis displays cell coverage for day 5 expressed in terms of percent of total area based on image area analysis.

After determining that the PCL-protein nanofiber scaffolds supported cellular proliferation and differentiation, the ability of the scaffolds to act as a biomaterial bridge and guide the orientation of neurite outgrowth was evaluated. Figure 6(a) displays a representative image of PC12 cells cultured on aligned PCL fibers used to study neurite orientation. The angles of the fiber axis and neurites were measured

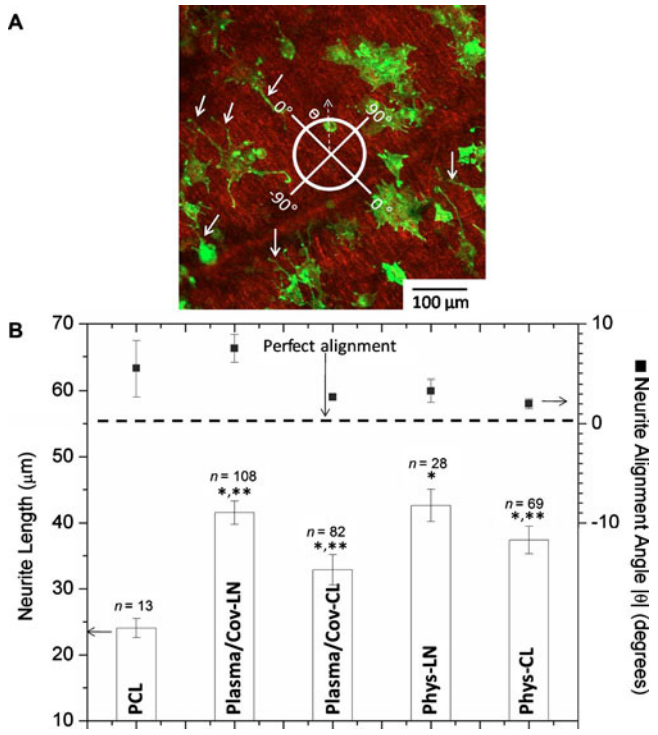

FIG. 6. (Color onlne) (a) Confocal scanning laser microscopy image of PC12 cells cultured on aligned PCL nanofibers with physically adsorbed collagen. Cells were cultured for 5 days. This image indicates the methodology used to measure neurite alignment with respect to fiber alignment. The fiber axis was set to 0° and the neurite angle (■) ranged between 0 and ±90°. Absolute values of angles were used to compute the results in (b). Arrows point out representative neurites that were measured. (b) Comparison of neurite alignment and outgrowth of PC12 cells cultured on aligned electrospun PCL fibers with physically adsorbed and covalently attached LN and CL after 5 days in culture. Data are expressed as mean ± standard error of the mean ($^{*}p<0.05$ compared to PCL fibers and $^{**}p<0.05$ compared to covalent-CL fibers). The right axis shows the average value of the neurite angle relative to the average fiber angle where the dashed line at $\theta=0$ indicates perfect alignment of neurites with fibers.

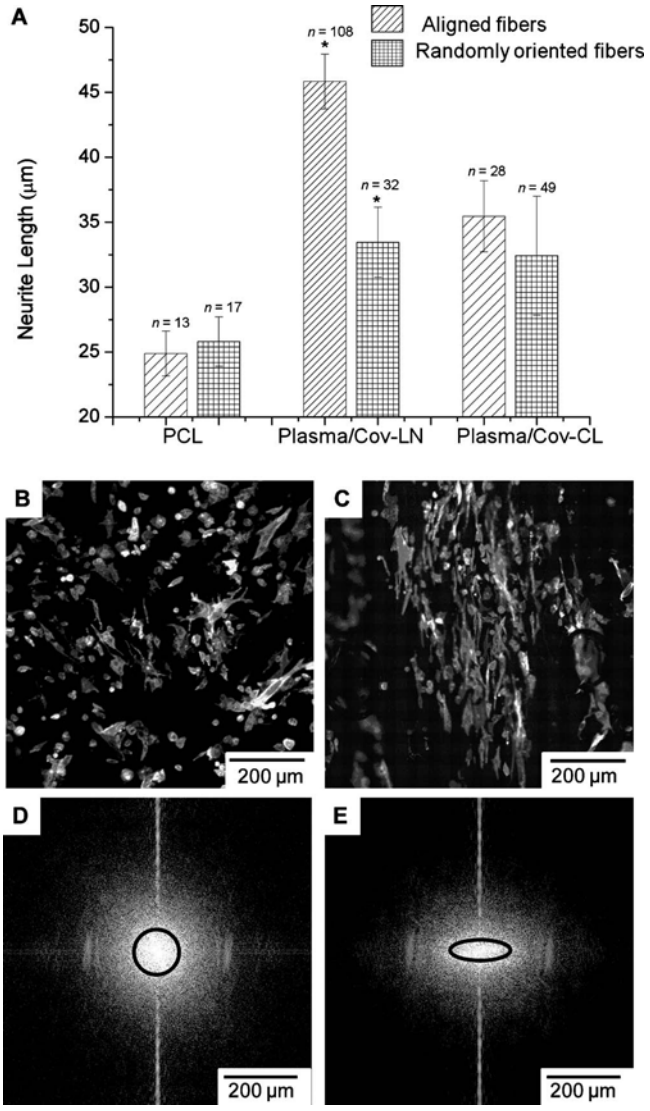

FIG. 7. (a) Neurite outgrowth of PC12 cells cultured on aligned and unaligned electrospun PCL fibers with covalently attached LN and CL. Data are expressed as mean ± standard error of the mean ($^{*}p<0.05$). [(b)–(d)] Confocal scanning laser microscopy images of PC12 cells on electrospun PCL fibers with covalently attached laminin. (b) Unaligned fibers, (c) aligned fibers, (d) FFT of (b), and (e) FFT of (c). Shapes superimposed in FFT images are meant to guide the eye and indicate horizontal elongation in (e) along the vertical principal alignment axis in (c), whereas FFT image (d) indicates no particular axis of alignment for neurites grown on the unaligned fibers in (b).

and averaged, and the absolute value of the difference was determined. As illustrated in Fig. 6(b), the surface chemistry had no affect on the neurite orientation, and native as well as protein modified PCL all successfully guided neurites along the fiber axis. The length of the neurites was affected by the surface chemistry, as discussed above.

C. Interaction of PC12 cells with unaligned PCL nanofibrous scaffolds

The effect of fiber orientation on cell viability was also examined (not shown), and no significant difference was observed between aligned fibers and unaligned fibers, indicating that fiber orientation had no effect on cellular proliferation. Neurite outgrowth on unaligned fibers was also evaluated and no significant difference was found between unmodified PCL unaligned and aligned fibers or covalent collagen PCL unaligned and aligned fibers [Fig. 7(a)]. The difference between unaligned and aligned fibers with covalently bound laminin was significant, which is in agreement with previous results that observed longer neurites on aligned fibers.[21] Wang *et al.* observed an increase in neurite length with fiber diameter, while Lee *et al.* saw no such effect for hippocampal neurons.[39,40] Thus, we did not select fiber diameter as a variable in these studies, since there seems to be no consensus for the effect of fiber diameter on neurite length, and because the fiber diameters here differed by only a factor of 2, with a fairly broad size distribution. As shown previously, fiber orientation was the more important factor in controlling neurite outgrowth.

Aspect ratios of the cells and neurites were also calculated (see supplemental data, Table I).[38] For these measurements, no significant difference was found between the unaligned and aligned fibers for any of the surface chemistries evaluated.

The lack of a significant difference between unaligned and aligned fibers for PCL and covalent collagen PCL could possibly be attributed to lower cell adhesion and absence of biochemical cues, and inefficiency of the protein coupling reaction, respectively. Calculations of full width at half maximum (FWHM) from radial pixel intensities of FFT images derived from the CLSM micrographs were attempted as done by Corey *et al.*, but due to the presence of the spherical cell bodies in the images and the relatively short neurites compared to the cell bodies, quantitatively significant differences between neurite orientation angle distributions for aligned and unaligned fibers were not observed.[11] Figures 7(b)–7(e) display representative CLSM and FFT images for PC12 cells cultured on PCL fibers with covalently bound laminin for 5 days. The overlaid shapes on the FFTs indicate the regions of highest pixel intensity. There is evidence of a principal axis of alignment for the cells and neurites grown on aligned fibers and the FFT has an elliptical band perpendicular to that axis, whereas the FFT from cells grown on unaligned fibers is more spherical, indicating no preferred orientation of cells and neurites.

D. Discussion

As mentioned previously, the major challenge in nerve regeneration is the ability to coax axons across injury sites and inhibitory scar regions in the nerve tissue. It has been shown that aligned fibers are able to control neurite outgrowth along the fiber axis. In this work, the degree of alignment between the fiber axis and the neurite axis was quantified and near perfect alignment between the two axes was observed (less than 7° difference). Unaligned fibers were also examined for their effects on neurite outgrowth, but as there was no principal fiber axis, quantification of the degree of alignment could not be calculated in the same manner as with the aligned fibers. Attempts to use FFTs of unaligned fibers CLSM images to correlate pixel intensity with orientation angles and determine the spread of orientation of the neurites (FWHM) failed to show a significant difference from aligned fibers. Corey *et al.* and others have been able to observe significant differences for dorsal root ganglion (DRG) neurons cultured on aligned fibers and unaligned fibers, but DRG neurite lengths were approximately 700 μm compared to approximately 40 μm for the PC12 cells used in this work.[11] The majority of the pixels in the image were composed of spherical PC12 cell bodies (10–20 μm in diameter) and thus dominated the pixel intensity pattern rather than the neurites, and hence it was difficult to find a quantifiable difference between PC12 cells cultured on aligned fibers and unaligned fibers, although the FFTs did show distinct patterns.

Thus, it was shown that the aligned nanofibers controlled the direction of neurite outgrowth, but in order to form a biomaterial bridge that can direct axons and also support tissue reconstruction, biological compatibility and cell-scaffold interaction also needed to be considered. It is well known that ECM proteins play an important role in cell adhesion, proliferation, and differentiation, among other cellular processes. Many researchers have reported enhanced cell adhesion by incorporation of ECM proteins onto nanofiber scaffolds. However, differences in adhesion, proliferation, and differentiation resulting from the attachment chemistries and direct comparisons between ECM proteins have been little examined. In this work, the effects of covalent versus physically adsorbed protein attachment were explored and the differences in PC12 cell adhesion and proliferation were not found to be significant. The difference in neurite outgrowth was significantly shorter for the covalently attached collagen fibers, but as discussed above, it was likely due to reduced coupling efficiency and hence lower protein content at the surface. Further research is needed to improve the coupling efficiency for collagen. The reaction has been tested at *p*H 8, and the at. % nitrogen doubled to 4%, but this was still substantially lower than that observed on the laminin and physically absorbed collagen fibers. Reactions above the pKa of the collagen protein (approximately 6.8) could potentially cause denaturation and this must be taken into account. Li *et al.* found that increased carboxyl content (in copolymer fibers composed of methylmethacrylate and acrylic acid) and a subsequent EDC coupling reaction led to longer neural stem cell process lengths due to increased protein attachment.[23] Thus, it could be difficult to make direct comparisons between surfaces with different amounts of protein, as the amount of protein and not just the type of protein and how it is bound to the surface affect cellular processes.

It was anticipated that the polyclonal bioavailability of the proteins in the bound versus physically adsorbed forms would be different because it was thought that the covalent binding of the protein could force it into a less active conformation. The immunoassay showed that this assumption was incorrect and a similar bioavailability was observed for both attachment mechanisms of laminin. Thus, covalent attachment via EDC coupling does not compromise the protein's polyclonal bioavailability and hence it is a suitable method to incorporate proteins onto fiber scaffolds. Covalent attachment could be highly beneficial for long-term cell culture studies and *in vivo* tissue regeneration as the protein would not desorb from the surface over time.[41–43]

Longer neurites were expected on the laminin modified fibers because laminin contains an IKVAV sequence known to influence neurite outgrowth. Neal *et al.* found that PC12 cells cultured on fibers electrospun from pure laminin were able to differentiate without NGF.[31] Possibly, the total amount of laminin and the number of IKVAV binding sites in the scaffold were too low to enhance neurite outgrowth over the collagen modified scaffolds, which is also known to enhance the biocompatibility of scaffolds. An analysis of total protein could be useful in better understanding this cell-scaffold interaction.

IV. SUMMARY AND CONCLUSIONS

Polycaprolactone nanofibers were prepared via electrospinning and subsequently modified with ECM proteins to improve biocompatibility. The effect of protein type, attachment chemistry, as well as fiber orientation on neuronlike

PC12 cell proliferation and differentiation were examined. Two ECM proteins, namely, collagen and laminin, were both physically adsorbed and covalently bound to PCL nanofibers and compared for their efficacy in enhancing proliferation and neurite outgrowth. There was no significant difference found for proliferation for any of the protein modified surfaces, and all showed similar proliferation compared to native PCL nanofibers. In addition, cells cultured on all of the protein modified fibers had significantly longer neurites than cells grown on unmodified PCL fibers. Cells grown on the covalently attached laminin, as well as physically absorbed laminin and collagen, had longer neurites than cells grown on covalently attached collagen. Further research is needed to determine whether the shorter neurites observed on covalently attached collagen fibers is due to reduced bioavailability of the collagen or reduced protein content on the fibers. Neurite orientation was found to be in near perfect alignment with the fiber axis for cells grown on aligned fibers, regardless of the surface chemistry. Neurites on unaligned fibers showed reduced fiber alignment based on FFTs of CLSM images, but a quantitative comparison proved difficult due to the relatively short neurite lengths compared to the cell bodies, the latter dominating the FFT pixel intensities. Neurite lengths on aligned fibers coupled with laminin were significantly longer than on unaligned fibers. The polyclonal bioavailability of laminin modified fibers was found to be identical for both covalently attached and physically adsorbed laminin, indicating that covalent attachment does not diminish the activity of the protein by changing its conformation to an unfavorable one. Thus, of the surface chemistries, proteins and fiber orientations examined, aligned PCL fibers with covalently bound laminin are the most promising scaffolds for nerve regeneration.

[1]R. V. Bellamkonda, Biomaterials **27**, 3515 (2006).
[2]X. J. Wen and P. A. Tresco, J. Biomed. Mater. Res. Part A **76A**, 626 (2006).
[3]L. J. Zhang and T. J. Webster, Nanotoday **4**, 66 (2009).
[4]C. E. Schmidt and J. B. Leach, Annu. Rev. Biomed. Eng. **5**, 293 (2003).
[5]J. M. Corey, D. Y. Lin, K. B. Mycek, Q. Chen, S. Samuel, E. L. Feldman, and D. C. Martin, J. Biomed. Mater. Res. Part A **83A**, 636 (2007).
[6]L. Yao, N. O'Brien, A. Windebank, and A. Pandit, J. Biomed. Mater. Res., Part B: Appl. Biomater. **90B**, 483 (2009).
[7]C. T. Chalfoun, G. A. Wirth, and G. R. D. Evans, J. Cell. Mol. Med. **10**, 309 (2006).
[8]R. Langer and J. P. Vacanti, Science **260**, 920 (1993).
[9]P. Sangsanoh, S. Waleetorncheepsawat, O. Suwantong, P. Wutticharoenmongkol, O. Weeranantanapan, B. Chuenjitbuntaworn, P. Cheepsunthorn, P. Pavasant, and P. Supaphol, Biomacromolecules **8**, 1587 (2007).
[10]T. B. Bini, S. J. Gao, T. C. Tan, S. Wang, A. Lim, L. B. Hai, and S. Ramakrishna, Nanotechnology **15**, 1459 (2004).
[11]J. M. Corey, D. Y. Lin, D. C. Martin, and E. L. Feldman, Ann. Neurol. **58**, S65 (2005).
[12]E. C. Tsai, P. D. Dalton, M. S. Shoichet, and C. H. Tator, Biomaterials **27**, 519 (2006).
[13]H. W. Ma, J. Hyun, Z. P. Zhang, T. P. Beebe, and A. Chilkoti, Adv. Funct. Mater. **15**, 529 (2005).
[14]R. L. Waddell, K. G. Marra, K. L. Collins, J. T. Leung, and J. S. Doctor, Biotechnol. Prog. **19**, 1767 (2003).
[15]H. Q. Cao, T. Liu, and S. Y. Chew, Adv. Drug Delivery Rev. **61**, 1055 (2009).
[16]S. G. Kumbar, R. James, S. P. Nukavarapu, and C. T. Laurencin, Biomed. Mater. **3**, 034002 (2008).
[17]A. Greiner and J. H. Wendorff, Angew. Chem., Int. Ed. **46**, 5670 (2007).
[18]W. J. Li, C. T. Laurencin, E. J. Caterson, R. S. Tuan, and F. K. Ko, J. Biomed. Mater. Res. **60**, 613 (2002).
[19]D. Li and Y. N. Xia, Adv. Mater. **16**, 1151 (2004).
[20]Z. M. Huang, Y. Z. Zhang, M. Kotaki, and S. Ramakrishna, Compos. Sci. Technol. **63**, 2223 (2003).
[21]J. W. Xie, M. R. MacEwan, X. R. Li, S. E. Sakiyama-Elbert, and Y. N. Xia, ACS Nano **3**, 1151 (2009).
[22]F. Yang, R. Murugan, S. Wang, and S. Ramakrishna, Biomaterials **26**, 2603 (2005).
[23]W. S. Li, Y. Guo, H. Wang, D. J. Shi, C. F. Liang, Z. P. Ye, F. Qing, and J. Gong, J. Mater. Sci.: Mater. Med. **19**, 847 (2008).
[24]D. R. Nisbet, L. M. Y. Yu, T. Zahir, J. S. Forsythe, and M. S. Shoichet, J. Biomater. Sci., Polym. Ed. **19**, 623 (2008).
[25]H. S. Yoo, T. G. Kim, and T. G. Park, Adv. Drug Delivery Rev. **61**, 1033 (2009).
[26]W. Mattanavee, O. Suwantong, S. Puthong, T. Bunaprasert, V. P. Hoven, and P. Supaphol, ACS App. Mater. Interfaces **1**, 1076 (2009).
[27]M. Y. Li, Y. Guo, Y. Wei, A. G. MacDiarmid, and P. I. Lelkes, Biomaterials **27**, 2705 (2006).
[28]L. Ghasemi-Mobarakeh, M. P. Prabhakaran, M. Morshed, M.-H. Nasr-Esfahani, and S. Ramakrishna, Biomaterials **29**, 4532 (2008).
[29]M. Li, M. J. Mondrinos, X. Chen, M. R. Gandhi, F. K. Ko, and P. I. Lelkes, J. Biomed. Mater. Res. Part A **79A**, 963 (2006).
[30]E. Schnell, K. Klinkhammer, S. Balzer, G. Brook, D. Klee, P. Dalton, and J. Mey, Biomaterials **28**, 3012 (2007).
[31]R. A. Neal, S. G. McClugage, M. C. Link, L. S. Sefcik, R. C. Ogle, and E. A. Botchwey, Tissue Eng. **15**, 11 (2009).
[32]L. A. Greene and A. S. Tischler, Proc. Natl. Acad. Sci. U.S.A. **73**, 2424 (1976).
[33]H. S. Koh, T. Yong, C. K. Chan, and S. Ramakrishna, Biomaterials **29**, 3574 (2008).
[34]C. E. Ayres, B. S. Jha, H. Meredith, J. R. Bowman, G. L. Bowlin, S. C. Henderson, and D. G. Simpson, J. Biomater. Sci., Polym. Ed. **19**, 603 (2008).
[35]S. Y. Chew, R. Mi, A. Hoke, and K. W. Leong, Biomaterials **29**, 653 (2008).
[36]E. D. Yildirim, R. Besunder, D. Pappas, F. Allen, S. Güceri, and W. Sun, Biofabrication **2**, 014109 (2010).
[37]M. P. Prabhakaran, J. Venugopal, C. K. Chan, and S. Ramakrishna, Nanotechnology **19**, 455102 (2008).
[38]See supplementary material at http://dx.doi.org/10.1116/1.3526140 for preparation and analysis details.
[39]B. Wang, M. E. Mullins, J. M. Cregg, C. W. McCarthy, and R. J. Gilbert, Acta Biomater. **6**, 2970 (2010).
[40]J. Y. Lee, C. A. Bashur, N. Gomez, A. S. Goldstein, and C. E. Schmidt, J. Biomed. Mater. Res. Part A **92A**, 378 (2010).
[41]S. K. Bhatia, L. C. Shriver-Lake, K. J. Prior, J. H. Georger, J. M. Calvert, R. Bredehorst, and F. S. Ligler, Anal. Biochem. **178**, 408 (1989).
[42]L. C. Shriver-Lake, B. Donner, R. Edelstein, K. Breslin, S. K. Bhatia, and F. S. Ligler, Biosens. Bioelectron. **12**, 1101 (1997).
[43]Z. H. Wang and G. Jin, J. Immunol. Methods **285**, 237 (2004).